Discovery of the actinoplanic acid pathway in *Streptomyces rapamycinicus* reveals a genetically conserved synergism with rapamycin

Received for publication, August 15, 2018, and in revised form, October 11, 2018 Published, Papers in Press, October 16, 2018, DOI 10.1074/jbc.RA118.005314

Peter Mrak[‡§1], **Philipp Krastel**[¶], **Petra Pivk Lukančič**[‡], **Jianshi Tao**[‖], **Dominik Pistorius**[¶], **and Charles M. Moore**[¶2]

From the [‡]*Novartis Technical Operations, Antiinfectives, SI-1234 Mengeš, Slovenia,* [¶]*Novartis Institutes for BioMedical Research, Novartis Campus, 4056 Basel, Switzerland,* [‖]*Genomics Institute of the Novartis Research Foundation, San Diego, California 92121, and* [§]*University of Ljubljana, 1000 Ljubljana, Slovenia*

Edited by Chris Whitfield

Actinobacteria possess a great wealth of pathways for production of bioactive compounds. Following advances in genome mining, dozens of natural product (NP) gene clusters are routinely found in each actinobacterial genome; however, the *modus operandi* of this large arsenal is poorly understood. During investigations of the secondary metabolome of *Streptomyces rapamycinicus*, the producer of rapamycin, we observed accumulation of two compounds never before reported from this organism. Structural elucidation revealed actinoplanic acid A and its demethyl analogue. Actinoplanic acids (APLs) are potent inhibitors of Ras farnesyltransferase and therefore represent bioactive compounds of medicinal interest. Supported with the unique structure of these polyketides and using genome mining, we identified a gene cluster responsible for their biosynthesis in *S. rapamycinicus*. Based on experimental evidence and genetic organization of the cluster, we propose a stepwise biosynthesis of APL, the first bacterial example of a pathway incorporating the rare tricarballylic moiety into an NP. Although phylogenetically distant, the pathway shares some of the biosynthetic principles with the mycotoxins fumonisins. Namely, the core polyketide is acylated with the tricarballylate by an atypical nonribosomal peptide synthetase–catalyzed ester formation. Finally, motivated by the conserved colocalization of the rapamycin and APL pathway clusters in *S. rapamycinicus* and all other rapamycin-producing actinobacteria, we confirmed a strong synergism of these compounds in antifungal assays. Mining for such evolutionarily conserved coharboring of pathways would likely reveal further examples of NP sets, attacking multiple targets on the same foe. These could then serve as a guide for development of new combination therapies.

Actinoplanic acids A and B are actinobacterial secondary metabolites first isolated from *Streptomyces* sp. MA7099 and *Actinoplanes* sp. MA7066 for their farnesyltransferase inhibitory activity (1). Actinoplanic acid A is a polyketide with a 30-membered carbon backbone, assembled from malonate, methyl malonate, and ethyl malonate units. It contains a unique tricarballylic acid–bridged structure, cyclizing a part of the polyketide into a double-ester lactone (2) (see Fig. 1*B*). In actinoplanic acid B, this structure remains acyclic due to the absence of the hydroxyl group on carbon 36 (3). Stereochemical characterization of these compounds has remained elusive to date due to the complex nature of the NMR spectra and the inability to obtain crystalline material that would permit X-ray studies (3). Despite their unique structural features, little attention has been devoted to actinoplanic acids after initial discovery and characterization of their bioactive properties (1). In these reports, actinoplanic acids A and B were found to be highly potent and selective competitive Ras farnesyl-protein transferase inhibitors (FTIs).[3] Limited structure-activity relationship observations suggest that the tricarballylic moieties and more specifically its free carboxylic groups are important for the biological activity of actinoplanic acids (3). Ras GTPase, one of the most prevalent oncogenes, is an important target in development of anticancer drugs (4), and although FTIs have not yielded approved therapies thus far, significant efforts are being invested to harness their potential (5). In addition, FTIs have been successfully used for the treatment of progeria and are being considered for the treatment of Alzheimer's disease and certain protozoan infections (6).

In contrast to the actinoplanic acids, which remain unexplored in their biosynthetic origin, the only other known natural products featuring a tricarballylate moiety, the fungal toxins fumonisins (7) (see Fig. 1*B*), have received significantly more attention. Encoded by 15 genes covering ~30 kb (8), the fumonisin biosynthetic pathway is initiated with the formation of a linear polyketide, which is assembled by an iterative type I polyketide synthase (PKS) (9). The nascent polyketide is

The authors declare that they have no conflicts of interest with the contents of this article.

This article was selected as one of our Editors' Picks.

This article contains Figs. S1–S15, Tables S1–S6, and Data Set S1.

The nucleotide sequence(s) reported in this paper has been submitted to the GenBank™/EBI Data Bank with accession number(s) QYCY00000000.

[1] To whom correspondence may be addressed: Novartis Technical Operations, Antiinfectives, Kolodvorska 27, SI-1234 Mengeš, Slovenia. Tel.: 386-1-721-7583; E-mail: peter.mrak@novartis.com.

[2] To whom correspondence may be addressed. Tel. 41-79-727-7876; E-mail: charles-1.moore@novartis.com.

[3] The abbreviations used are: FTI, farnesyl-protein transferase inhibitor; PKS, polyketide synthase; NRPS, nonribosomal peptide synthetase; NP, natural product; APL, actinoplanic acid; TOR, target of rapamycin; SARP, Streptomyces antibiotic regulatory protein; TCA, tricarboxylic acid; HRMS, high-resolution MS; ACP, acyl carrier protein; AT, acyltransferase; CCR, crotonyl-CoA reductase; PCP, peptidyl carrier protein; A, adenylating; C, condensation; PDB, potato dextrose broth; TORC, TOR complex; CDS, coding sequence; *permE**, *ermE** promoter; UPLC, ultraperformance LC; ESI, electrospray ionization; PDA, potato dextrose agar.

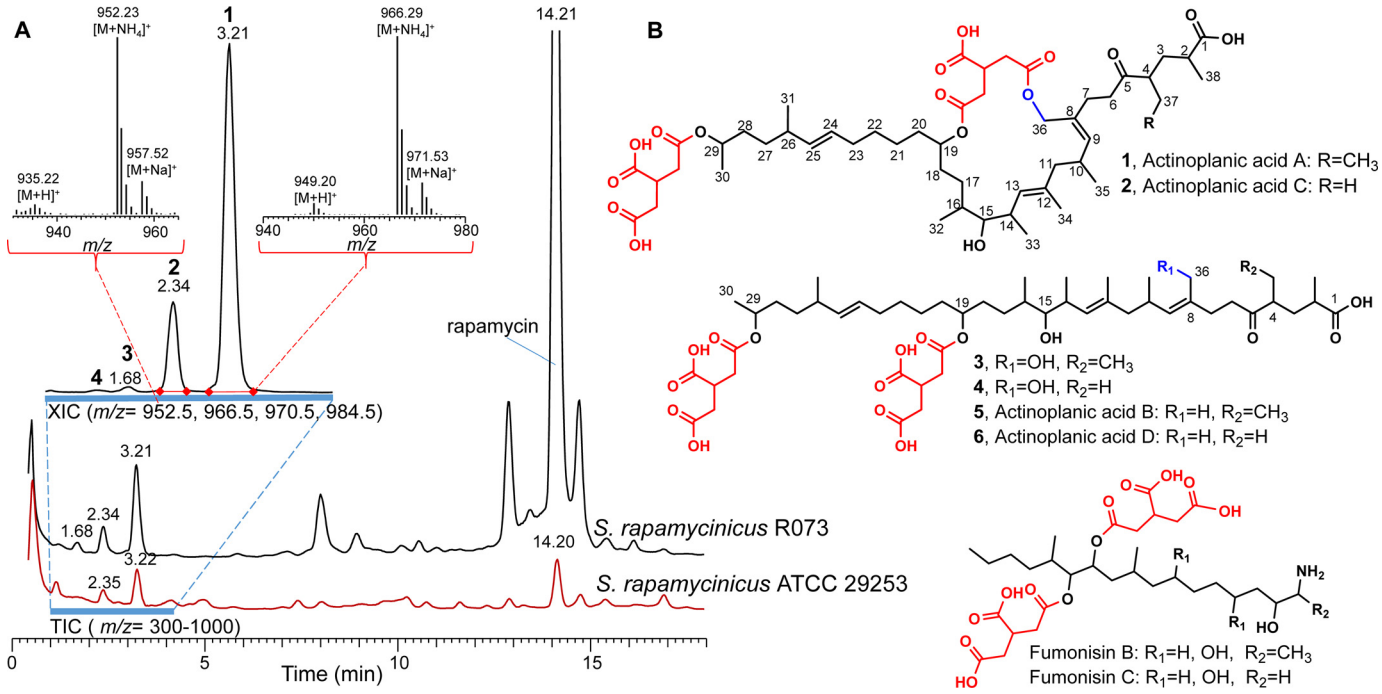

Figure 1. LC-MS chromatogram of *S. rapamycinicus* ATCC 29253 and *S. rapamycinicus* R073 culture extracts. *A*, full-scan LC-MS data in the *m/z* range 300–1000 with normalized intensities on the *vertical axis*. Extracted (*XIC*) chromatograms show the major actinoplanic acid species (**1**, **2**, **3**, and **4**). Mass spectra of actinoplanic acid A (**1**) and actinoplanic acid C (**2**) are shown. Rapamycin-related compounds populate the *right* part of the chromatogram. HRMS: **1**, $C_{51}H_{80}O_{16}$; measured $[M + NH_4]^+$ 966.57913; calculated $[M + NH_4]^+$ 966.579014; Δ 0.12 ppm. **2**, $C_{50}H_{78}O_{16}$; measured $[M + NH_4]^+$ 952.56320; calculated $[M + NH_4]^+$ 952.563364; Δ −0.17 ppm. **3**, $C_{51}H_{82}O_{17}$; measured $[M + NH_4]^+$ 984.58960; calculated $[M + NH_4]^+$ 984.589579; Δ 0.02 ppm. **4**, $C_{50}H_{80}O_{17}$; measured $[M + NH_4]^+$ 970.57431; calculated $[M + NH_4]^+$ 970.573929; Δ 0.39 ppm. *B*, structures of actinoplanic acids found in *S. rapamycinicus* are depicted on the *far right*. For comparison, the structure of fungal toxins fumonisins B and C is also shown. The tricarballylic moieties are colored *red*.

released by a unique mechanism, involving a condensation reaction with alanine or glycine to form a full-length, free, linear intermediate (10), which is then modified further by a series of post-PKS enzymes. Perhaps the most interesting among these is the nonribosomal peptide synthetase (NRPS)-catalyzed acylation of the intermediate, resulting in an ester with two tricarballylic acids (11). The origin of the tricarballylate has also been investigated, revealing an interesting reduction of aconitic acid while thioester-bound to the NRPS complex (12).

The actinomycete *Streptomyces rapamycinicus*, initially classified as *Streptomyces hygroscopicus*, is best known for its production of the immunosuppressant rapamycin (13). Following the discovery of rapamycin's inhibition of TOR complex signaling, this macrolide has proven an invaluable asset for cell biology research as well as clinical use (13). Because of its medical and industrial importance, significant efforts have been invested into understanding the biosynthesis of rapamycin and improving the yield from *S. rapamycinicus* (13). In addition to rapamycin, this organism has been reported to produce other secondary metabolites, including elaiophylin and nigericin (14). Recently, the genome sequence of *S. rapamycinicus* ATCC 29253 was published, proving to be one of the largest actinobacterial genomes, rich in natural product (NP) biosynthetic gene clusters (15).

In this study, we report accumulation of actinoplanic acid A (2) and its novel demethyl analogue, which we have designated actinoplanic acid C, in the fermentation broth of *S. rapamycinicus* ATCC 29253. These compounds are unrelated to any of the secondary metabolites previously reported from this microorganism. Through genome mining, using PKS domain architecture prediction tools, we identified the putative actinoplanic acid (APL) biosynthetic gene cluster. We further describe the APL biosynthetic pathway based on *in silico* analysis and experimental evidence, which revealed the key biochemical steps. CRISPR genome editing tools (16) were developed in house for this organism and applied to the dissection of the pathway. Most intriguing are the post-PKS steps, especially the mechanism for acylation of the nascent polyketide with tricarballylic moieties, which resembles the fumonisin biochemistry in the involvement of an ester-forming NRPS and the accompanied reduction of the tricarboxylic acid (TCA) intermediate.

Furthermore, we have identified the APL cluster in other bacterial genomes, without exception in the presence of the rapamycin pathway. Taking into account the biochemical similarities and genetic differences, both between the bacterial representatives and compared with fumonisins, we discuss the evolutionary implications. Among these, the most notable example is our discovery of a significant synergistic effect in antifungal activity of rapamycin and actinoplanic acid A, unveiling nature's strategy to attack multiple targets on the same foe. Our findings invite important questions in the quest for new natural compounds of medicinal value. Namely, how frequently have similar genetically conserved synergies evolved in secondary metabolism, and how can we identify potential synergistic compounds at the primary DNA sequence level?

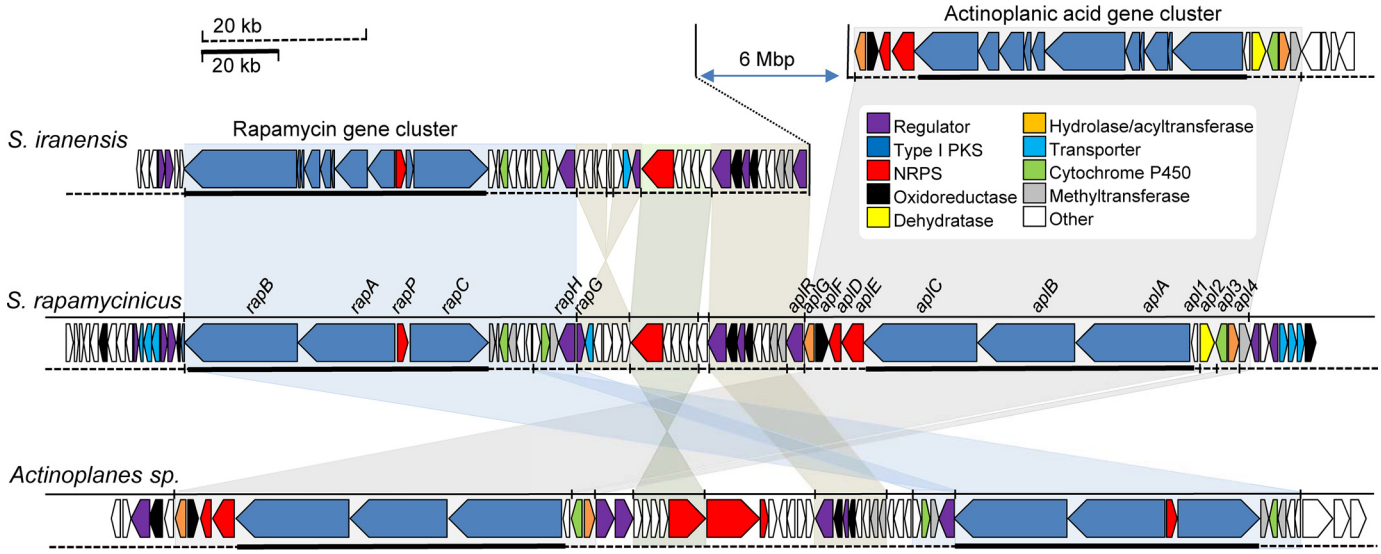

Figure 2. Genetic organization and synteny of rapamycin and actinoplanic acid gene clusters in genomes of the known rapamycin producers. Genomic loci encoding the rapamycin and actinoplanic acid clusters of *S. iranensis* HM35, *Streptomyces rapamycinicus* ATCC 29253, and *Actinoplanes* sp. N902-109 were compared. The scale of the large PKS genes is compressed 2-fold. The *S. rapamycinicus* APL gene cluster is labeled with gene designations. CDS locus tags, as found in the deposited genome annotations, are listed in Table S1.

Results and discussion

Identification of actinoplanic acids in S. rapamycinicus

LC-MS analysis of *S. rapamycinicus* ATCC 29253 cultures revealed a compound with m/z $[M + NH_4]^+$ 966.5 in the polar section of the chromatogram (Fig. 1*A*). High-resolution MS (HRMS) suggested a molecular formula of $C_{51}H_{80}O_{16}$, corresponding to actinoplanic acid A (**1**). We also identified a second compound (1:5 ratio compared with **1**) with m/z $[M + NH_4]^+$ 952.5 and a proposed molecular formula of $C_{50}H_{78}O_{16}$. This corresponds to a novel actinoplanic acid demethyl analogue, which we designated actinoplanic acid C (**2**). Both compounds were isolated to yield white amorphous solids. 1D and 2D NMR was applied to confirm the chemical structures (Fig. 1*B* and Figs. S1 and S2). In addition, previously undescribed open-chain variants of both compounds were found with m/z $[M + NH_4]^+$ 970.5 and m/z $[M + NH_4]^+$ 984.5 (**4** and **3**, respectively) in the same 1:5 ratio (Fig. 1*A*). The HRMS data agree with the proposed molecular formulas $C_{50}H_{80}O_{17}$ and $C_{51}H_{82}O_{17}$, respectively. The levels of these compounds were 2 orders of magnitude lower compared with **1** and **2**. Nevertheless, a suitable amount of **3** could be isolated to allow structure confirmation by NMR (Fig. S3). Only traces of actinoplanic acid B (**5**; m/z $[M + NH_4]^+$ 954.5) and its novel demethyl analogue, actinoplanic acid D (**6**; m/z $[M + NH_4]^+$ 968.5) were found at the limit of detection. A similar distribution of actinoplanic acid species, in somewhat higher overall levels, was observed from a rapamycin producer, *S. rapamycinicus* R073, isolated from ATCC 29253 (Fig. 1*A*).

Sequence analysis of the S. rapamycinicus APL gene cluster

The genome sequence of *S. rapamycinicus* ATCC 29253 (15) was analyzed with antiSMASH 3.0 (17), revealing a gene cluster with PKS domain logic and predicted enzymatic features that correspond well to the structural properties of actinoplanic acids. Similarity searches in the nonredundant databases revealed putative APL clusters in two other genomes, namely *Streptomyces iranensis* HM35 (18) and *Actinoplanes* sp. N902-109 (19), and were used comparatively to roughly frame the cluster (Fig. 2 and Table S1). To improve the gene calling and overall quality of the data, we resequenced the *S. rapamycinicus* ATCC 29253 using PacBio RS II technology (GenBank™ accession number QYCY00000000).

The APL genes of *S. rapamycinicus* show a typical type I PKS cluster organization (Fig. 2). The core of the cluster is composed of three large, modular PKS ORFs (*aplA*, *aplB*, and *aplC*) followed immediately downstream by two ORFs (*aplD* and *aplE*), collectively encoding components of a single-module NRPS. Next are a short-chain reductase (*aplF*) and a putative α/β-fold hydrolase/acylase (*aplG*). Additionally, downstream of *aplG*, a putative SARP transcriptional regulator was identified that is not conserved in the other two organisms.

Upstream of the PKS ORFs is a freestanding acyl carrier protein (ACP) (*apl1*) followed by a putative 2-methylcitrate dehydratase (*apl2*) and a CYP450 (*apl3*). This organization is conserved in *S. rapamycinicus* and *S. iranensis* but not in the *Actinoplanes* sp., which is devoid of the dehydratase gene. In all three clusters, an α/β-fold hydrolase/acylase is found next to the CYP450. In the *S. rapamycinicus* and *S. iranensis* clusters, a putative SAM-dependent methyltransferase is encoded next, whereas in *Actinoplanes* sp. this gene appears to be absent.

aplA, aplB, and aplC encode the thiotemplate for actinoplanic acid core polyketide

Analysis of the PKS domain architecture by antiSMASH revealed a 15-module PKS encoded within *aplA*, *aplB*, and *aplC*. The PKS domain composition and extender prediction fit well to the structural properties of the core polyketide (Fig. 3*A*). As is often the case with modular type I PKS, there are several predicted dehydratase domains within the PKS that need to be inactive to yield the actinoplanic acid structure. Specifically, this is observed with modules 2, 7, and 9. Similarly, the ketoreductase domain in module 14 is apparently inactive. Beyond module 15, remnants of an additional module can be observed,

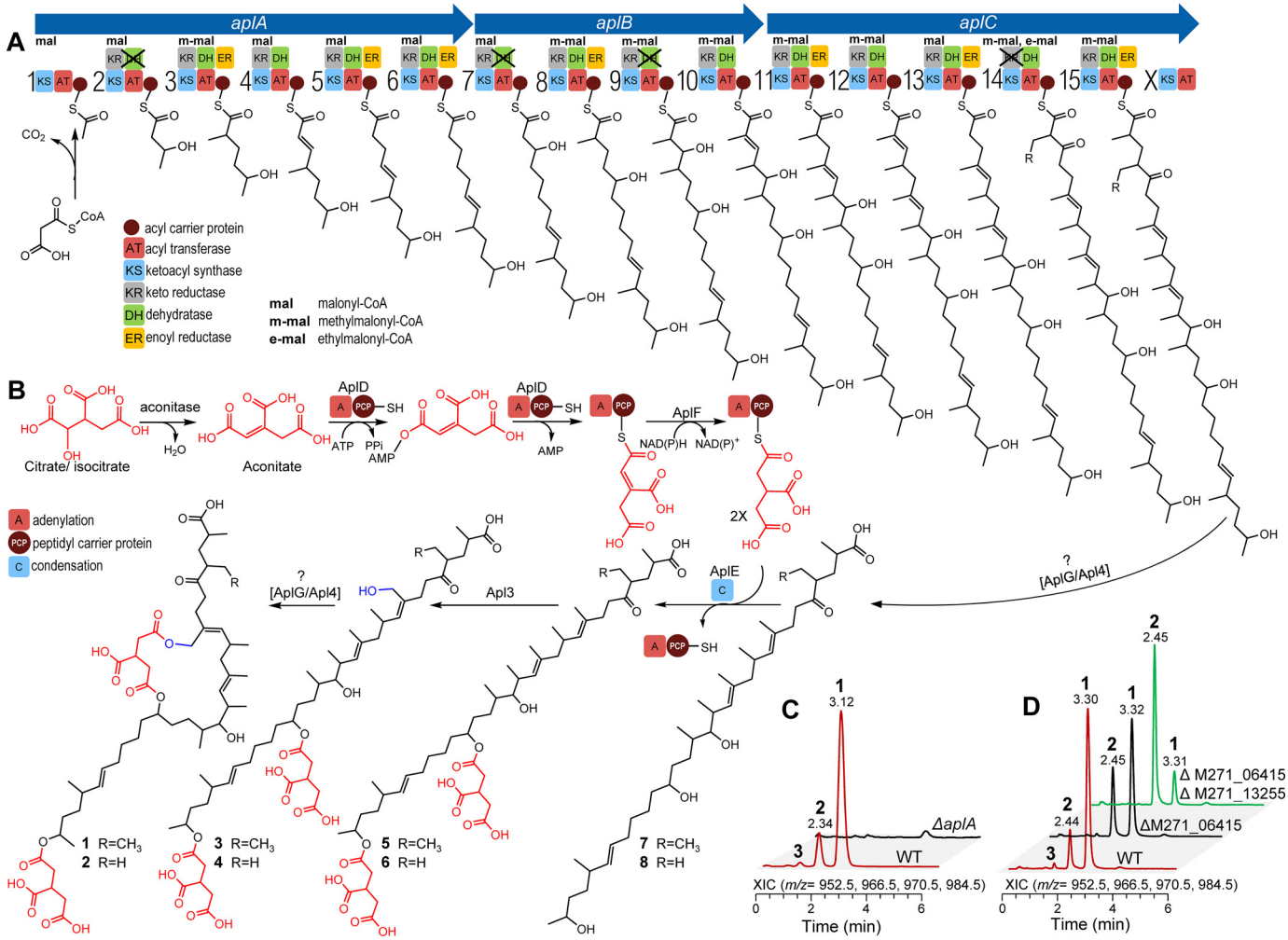

Figure 3. The proposed biosynthesis of actinoplanic acids in *S. rapamycinicus*. *A*, PKS assembly. Extender unit utilization and polyketide condensation sequence as derived from the bioinformatics prediction and structural properties of actinoplanic acid are shown. Each module is numbered and depicted with the encoded catalytic domains. The domains predicted to be inactive are *crossed out*. *B*, post-PKS sequence. The proposed NRPS-catalyzed acylation with tricarballylate side chains resulting in the double-lactone structure of **1** and **2** is shown. *C*, phenotype of *S. rapamycinicus* Δ*aplA* mutant. Extracted LC-MS chromatograms (*XIC*), with normalized intensities on the *vertical axis*, show the major actinoplanic acid species (**1**, **2**, **3**, and **4**) in *S. rapamycinicus* R073 (WT) and *S. rapamycinicus* R073 Δ*aplA*. *D*, phenotypes of *S. rapamycinicus* ΔCCR mutants. Extracted chromatograms (*XIC*), with normalized intensities on the *vertical axis*, show the major actinoplanic acid species (**1**, **2**, **3**, and **4**) in *S. rapamycinicus* R073 (WT), *S. rapamycinicus* R073 ΔM271_06415, and *S. rapamycinicus* R073 ΔM271_06415 ΔM271_13255.

indicated by the presence of a ketosynthase domain and an acyltransferase (AT) domain, but in the absence of an ACP as well as any of the reductive loop domains. Based on the conserved QSSSLV amino acid motif (20) in the ketosynthase domain of the loading module, we propose that the starter unit is obtained from malonyl-CoA, which is decarboxylated upon initiation of PKS synthesis.

We introduced a frameshift deletion into the 5′ end of *S. rapamycinicus aplA* gene and analyzed the mutant cultures by LC-MS. Complete absence of actinoplanic acids was observed (Fig. 3*C*), whereas the accumulation of other secondary metabolites remained largely unaffected (Fig. S4*A*). This confirms that the described PKS system is responsible for the biosynthesis of actinoplanic acids.

Actinoplanic acid PKS module 14 is promiscuous, incorporating either ethylmalonyl-CoA or methylmalonyl-CoA

Isolation of the novel actinoplanic acid C, having a methyl substituent at carbon 4 instead of an ethyl moiety, led us to assume that there is a level of promiscuity associated with the AT domain of module 14. Promiscuity of AT domains is frequently observed with various type I PKS products (21). In these cases, the rate of incorporation of a certain extender-CoA moiety largely depends on relative availability of the competing substrates from the cellular pool. Moreover, by feeding of synthetic extender–*N*-acetylcysteamine analogues in the absence of cluster-encoded biosynthesis of suitable extenders, this promiscuity can be fully exploited to dictate exclusive production of polyketide products with the desired substituents (22).

To reduce ethylmalonyl-CoA levels in the cellular pool and measure the consequent relative changes in the amounts of **1** *versus* **2** in the cultures, we targeted the crotonyl-CoA reductase (CCR) genes of *S. rapamycinicus*. Several highly conserved homologues were found in the genome. Two instances (M271_06415 and M271_13255) were comparatively highly expressed according to quantitative PCR analysis. Sequence analysis of the genomic context revealed that M271_06415 is located in the elaiophylin gene cluster, a biosynthesis path-

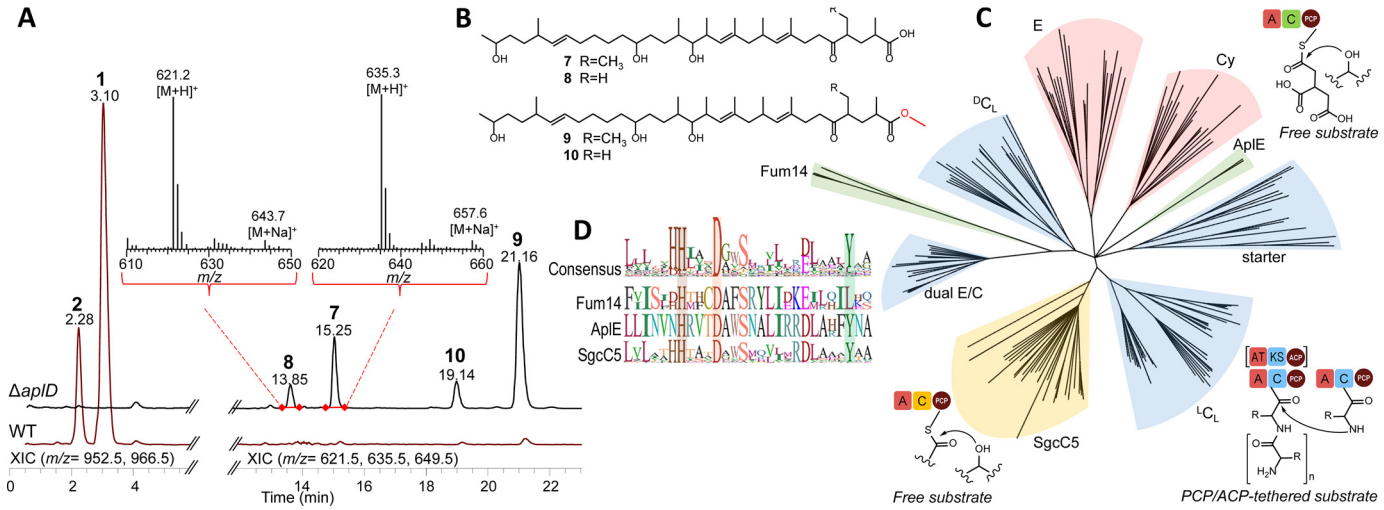

Figure 4. Phenotype of the *S. rapamycinicus aplD* deletion mutant. *A*, extracted LC-MS chromatograms (*XIC*) show the major actinoplanic acid species (**1** and **2**) and the core PKS intermediates in *S. rapamycinicus* R073 (WT) and *S. rapamycinicus* R073 Δ*aplD*. Normalized intensities are shown on the *vertical axis*. Mass spectra of **7** and **8** are shown. *B*, the proposed structures of **7**, **8**, **9**, and **10** are based on comparative HRMS/MS data with analogues derived synthetically from authentic actinoplanic acid samples (Fig. S7). HRMS: **7**, $C_{39}H_{70}O_6$; measured $[M + H]^+$ 635.52426; calculated $[M + H]^+$ 635.525065; Δ −0.64 ppm. **8**, $C_{38}H_{68}O_6$; measured $[M + H]^+$ 621.50867; calculated $[M + H]^+$ 621.509415; Δ −0.55 ppm. **9**, $C_{40}H_{72}O_6$; measured 649.54022; calculated 649.540715; Δ −0.15 ppm. **10**, $C_{39}H_{70}O_6$; measured 635.52484; calculated 935.525065; Δ 0.27 ppm. *C*, approximately maximum-likelihood, bootstrapped phylogenetic tree of various subtypes of condensation proteins/domains (see Fig. S8 and Data Set S1 for details) with schematic mode of action for assembly line C domains (*blue*) compared with ester-forming C domains (*yellow* and *green*) acting on nontethered substrates. *D*, active site motif conservation (see Fig. S8 and Data Set S1 for details). Multiple alignments were made from the complete dataset from C (consensus), five Fum14 analogues from *Fusarium* and *Aspergillus*, the three known AplE homologues, and the ester-forming clade surrounding SgcC5.

way known to utilize ethylmalonyl-CoA extender units (14, 23). The second CCR (M271_13255) is positioned next to a putative ethylmalonyl-CoA mutase, which likely makes it a part of the generally conserved ethylmalonyl-CoA pathway (24). An M271_06415 in-frame deletion mutant was constructed, and cultures were analyzed by LC-MS. The levels of extender-CoA in the CCR mutant were not directly measured; however, lower relative levels of elaiophylin and of the recently described rapamycin analogues, the homorapamycins (25), indicated a reduction in the ethylmalonyl-CoA cellular pool. Indeed, the ratio of **1** *versus* **2** changed from 5:1 in the WT strain to 2:1 in the M271_06415 mutant, whereas the sum of both remained at similar levels. When a double M271_06415,M271_13255 mutant was investigated, the change in the ratio was even more pronounced, inverting from 5:1 to 1:5 (Fig. 3*D* and Fig. S5).

These results imply that the outcome of the APL pathway depends on the cellular extender-CoA pool composition. Moreover, with the absence of cluster-encoded CCR, an inter-pathway substrate supply is indicated, not only for actinoplanic acid but also for the rapamycin pathway. The latter is reflected in reduced production of the homorapamycins that was imposed by the CCR mutations. Despite this lack of self-sufficiency in ethylmalonyl-CoA supply, actinoplanic acid A is most likely the true end product of the pathway because the accumulation of demethyl congeners in *S. rapamycinicus* seems to be an exception among the known producers of actinoplanic acids (1).

Cluster-encoded NRPS initiates the first of the post-PKS modifications, the acylation with tricarballylic acid

The *aplD* and *aplE* genes are found in the APL cluster immediately downstream of the PKS core genes and are predicted to contain components of a single-module NRPS: *aplD* encodes an adenylating (A) domain and peptidyl carrier protein (PCP), whereas the *aplE* encodes a free-standing condensation (C) domain (Table S1). The coding domains are overlapping and appear to be organized into a bicistronic operon. An in-frame deletion of *aplD* in *S. rapamycinicus* resulted in loss of actinoplanic acid production according to LC-MS analysis. Instead, the bare PKS products **7** and **8** with *m/z* $[M + H]^+$ 635.5 and 621.5, respectively, were found to accumulate in the cultures together with their respective methyl esters, **9** and **10** (Fig. 4*A*). These intermediates, which again differ in the presence of either a methyl or ethyl group on carbon 4, were found in the same 5:1 ratio that can be observed between **1** and **2** in the WT strain. Identical results were obtained with an *aplE* in-frame deletion mutant (Fig. S6). **9** and **10** readily hydrolyzed to yield **7** and **8** under alkaline conditions (Fig. S7). We were also able to obtain **7** and **8** by alkaline hydrolysis of respective actinoplanic acids **5**, **6**, **11**, and **12**. Structures of **7**, **8**, **9**, and **10** were then confirmed by comparative HRMS/MS fragmentation of these different sources (Fig. S7).

The methyl esterification of the PKS backbone is unexpected because no trace of it can be found on any other actinoplanic acid species. These results may imply a pathway nonrelevant methylation event, with the acting methyltransferase being selective toward nonacylated PKS intermediates. Significant differences in charge and polarity brought by the acylation could very well support such selectivity. A putative class I SAM-dependent methyltransferase is encoded at the border of the *S. rapamycinicus* APL cluster (*apl5*), and members of this superfamily have been known to catalyze formation of methyl esters (26–28). Because *apl5* is not conserved in the clusters of all three hosts, we presumed that this gene is unlikely to be of critical importance for the pathway. Therefore, experimental

data to support its role or the role of the observed methylation are not available at this time.

In *trans* complementation of the mutations in *aplD* and *aplE* by a chromosomally integrated copy of *aplDE* under control of the strong *ermE** promoter reversed the mutant phenotype back to normal actinoplanic acid production with concomitant near disappearance of **7**, **8**, **9**, and **10** (Fig. S6). This confirms that the tricarballylate acylation of the PKS intermediate is catalyzed by an unusual ester-forming NRPS activity encoded by *aplD* and *aplE*.

Typically, NRPS and hybrid PKS–NRPS complexes function as chain elongation assembly lines. The growing chain is tethered with the terminal carboxylic group to the ACP/PCP of the module last in operation. This keeps the carboxylic group of the growing chain activated for condensation with the extender, which is waiting, also thioester-bound, on the next module in line (Fig. 4*C*). Thus, the direction of the chain elongation is defined (29). In contrast, the NRPS of the APL pathway has a function in post-PKS ornamentation, acting on positions distal to the terminal carboxylic group of the core polyketide (Fig. 4*C*). This atypical activity does not require the nascent polyketide to remain phosphopantetheinyl-bound during the acylation. Significant accumulation of the full-length, free intermediate in the *aplD* and *aplE* mutants indicates that the polyketide backbone can be efficiently released from the PKS without being acylated. Small amounts of **7**, **8**, **9**, and **10** can be also be detected in the WT cultures (Fig. 4*A*). Considering all the above, it is highly likely that AplD/AplE NRPS is acting on the released polyketide intermediate. Based on the domain prediction, the APL PKS seems to lack a release thioesterase domain; instead, one of the conserved hydrolases encoded within the cluster (*aplG* or *apl4*) may be involved in this release.

We attempted to confirm acylation of the free core polyketides **7** and **8** by feeding them to cultures of *S. rapamycinicus* Δ*aplA*, harboring an additionally integrated copy of *aplDE*. Judging from the complementation experiments described above (Fig. S6), this construct should provide efficient expression of the NRPS. Despite several attempts, which were extended to *in vitro* experiments using cell-free extracts of the above cultures in the presence of various TCA substrates and ATP, we failed to obtain convincing results. The likely reason is the poor solubility of intermediates **7** and **8** in an aqueous environment at mild conditions, which was confirmed by the complete absence of **7**, **8**, **9**, and **10** in samples of *in vitro* experiments as well as in intact or disrupted cultures of *S. rapamycinicus* Δ*aplD* unless an organic solvent was used for extraction (Fig. S9).

Examples of ester-forming NRPS systems are scarce (30), and the APL pathway therefore adds to a small, but growing list of secondary metabolite enzymes possessing this activity. Incidentally, the first ester-forming NRPS described, Fum10/Fum14, catalyzes the tricarballylate esterification in the fumonisin pathway (11, 31). Fum14, which encodes a C domain and PCP, has been shown to act on a nontethered PKS intermediate *in vitro* (11). Recently, another representative of these free-standing, ester-forming C proteins was examined in detail (32). The SgcC5, involved in the biosynthesis of streptomycetal C-1027 enediyne chromophore (33), was also confirmed to act by acylation of a free substrate. Based on phylogenetic relations, the authors propose a new family of ester-forming C enzymes, which constitute a distinctive clade with SgcC5 and possess a signature HH*XXX*DX_{14}Y motif in the active site (32). Reusing input data of this study, we positioned the Fum14 and the AplE homologues into the phylogenetic tree of NRPS C domains. Interestingly, the tricarballylic acid–transferring enzymes do not follow the proposed conserved active site rule or share phylogenetic relations. Instead, these proteins form divergent clades, one containing the Fum14 orthologues and the other containing the three known AplE orthologues (Fig. 4, *C* and *D*, and Fig. S8).

Origin of the tricarballylic acid

In fumonisin biosynthesis, the starting block for the synthesis of the tricarballylate side chains originates from the TCA cycle. A specific mitochondrial exporter, Fum11, supplies *cis*-aconitate to the fumonisin pathway (34). The substrate for the NRPS A domain (11) is thereby sequestered from the highly active, reversible mitochondrial aconitase by action of this transporter. An analogous mechanism was proposed for supply of *cis*-aconitate to itaconate biosynthesis in *Aspergillus terreus* (35). In bacteria, subcellular compartmentalization is absent; therefore, the starting block for the tricarballylate moiety in the APL pathway could be directly supplied from the TCA cycle. Interestingly, just upstream of the actinoplanic acid PKS ORFs in the *S. rapamycinicus* genome, we have found a putative methylcitrate dehydratase– encoding gene (MmgE/PrpD superfamily), *apl2*. In addition to methylcitrate, certain bacterial methylcitrate dehydratases can also catalyze dehydration of citrate and isocitrate at somewhat lower rates. In contrast to aconitases, they are unable to rehydrate the *cis*-aconitate and related nonsaturated compounds (36). Contrary to our suspicions, an in-frame deletion of *apl2* in *S. rapamycinicus* proved noncritical for the APL pathway under various conditions tested (Fig. S10) and was not investigated further.

By drawing parallels to fumonisin biosynthesis and presuming that *cis*-aconitate originating from the TCA cycle is the starting block for the acylation, it is clear that a saturation step is needed at some point to yield the tricarballylic groups of the actinoplanic acids. Immediately adjacent to the *aplD*/*aplE* pair, we have located a putative NAD(P)H-dependent short-chain reductase gene, *aplF*. A similarity search and conserved domain analysis predicted that AplF is most closely related to enoyl-ACP reductases and 3-oxoacyl-ACP reductases involved in fatty acid and polyketide biosyntheses. Interestingly, the gene is in opposite orientation to *aplD*/*aplE* and therefore transcribed independently (Fig. 2).

An in-frame deletion of *aplF* resulted in loss of actinoplanic acid production. Instead, a group of new compounds, **11** and **12**, was found to accumulate with *m*/*z* $[M + NH_4]^+$ 964.5 and 950.5. Detailed investigation with HRMS confirmed molecular formulas of $C_{51}H_{78}O_{16}$ and $C_{50}H_{76}O_{16}$, revealing that the new compounds are tetradehydro analogues of **5** and **6**, respectively. More specifically, these compounds have aconitic instead of tricarballylic acid incorporated at both of the expected positions. In total, eight chromatographically separated isomers

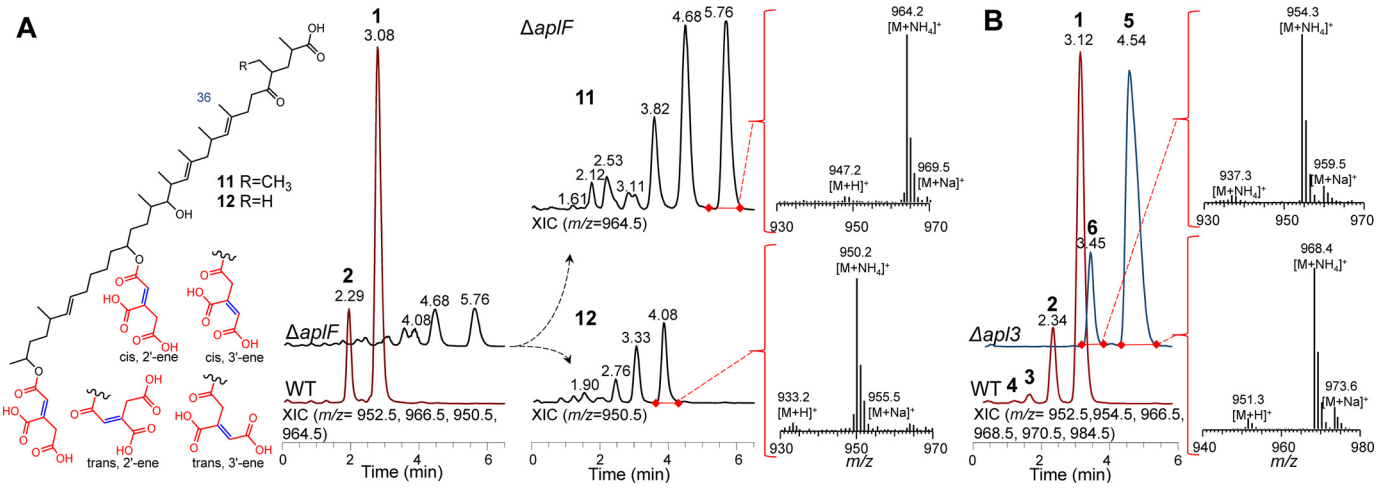

Figure 5. Phenotype of the *S. rapamycinicus aplF* deletion mutant. *A*, extracted LC-MS chromatograms (*XIC*), with normalized intensities on the *vertical axis*, show the major actinoplanic acid species (**1** and **2**) and the isomers of the nonsaturated analogues of actinoplanic acids B and D (**11** and **12**) in *S. rapamycinicus* R073 and *S. rapamycinicus* R073 Δ*aplF*. Mass spectra are from the largest extracted peak for each, **11** and **12**, and were found representative for all other peaks. HRMS: **11**, $C_{51}H_{78}O_{16}$; measured $[M + NH_4]^+$ 964.56298; calculated $[M + NH_4]^+$ 964.563364; Δ −0.39 ppm. **12**, $C_{50}H_{76}O_{16}$; measured $[M + NH_4]^+$ 950.54733; calculated $[M + NH_4]^+$ 950.547714; Δ −0.40 ppm. *B*, deletion of *apl3* results in a shift to production of actinoplanic acids B and D (5, 6). Extracted chromatograms (*XIC*), with normalized intensities on the *vertical axis*, show the major actinoplanic acid species (**1**, **2, 3, 4, 5**, and **6**) in *S. rapamycinicus* R073 (WT) and *S. rapamycinicus* R073 Δ*apl3*. Mass spectra of **5** and **6** are given on the *right*. HRMS: **5**, $C_{51}H_{82}O_{16}$; measured $[M + NH_4]^+$ 968.59425; calculated $[M + NH_4]^+$ 968.594664; Δ: −0.43 ppm. **6**, $C_{50}H_{80}O_{16}$; measured $[M + NH_4]^+$ 954.57867; calculated $[M + NH_4]^+$ 954.579014; Δ −0.36 ppm.

were found for each, **11** and **12** (Fig. 5*A*). This abundance of isomers is presumably due to the ability of the aconitic acid moiety to act as a conjugated system, allowing spontaneous double bond translocation (12). The possible isomers therefore include the geometric and regioisomers for each of the aconityl side chains, that is the *trans*/*cis* and the 2′-ene/3′-ene translocation. Alkaline hydrolysis of **11** and **12** isomers gave single peaks of **7** and **8,** respectively (Fig. S7). This, together with the HRMS data, confirms the structures of **11** and **12** as well as the assumption that the isomerization is occurring on the aconityl moieties. In *trans* complementation of the mutation with the *aplF* expressed under control of *ermE** promoter (p*ermE**) partially reversed the phenotype as indicated by the presence of actinoplanic acids **1** and **2** in the fermentation cultures (Fig. S11).

The above results resemble the phenotype obtained when *fum7* of the fumonisin biosynthetic pathway is blocked (12) and confirm the reductive function of AplF. These data are insufficient, however, to determine at which point in the post-PKS sequence the reduction of aconityl moieties takes place, *i.e.* on the free aconitic acid, the aconityl-PCP, or **11** and **12.** Based on similarity, AplF can most accurately be described as an enoyl-ACP reductase, thereby requiring a thioester-bound substrate such as acyl-ACP (PCP) or acyl-CoA for activity (37). This excludes the aconityl esters **11** and **12** or the free aconitic acid as likely substrates for the AplF. It is evident from the results that the AplD/AplE NRPS is able to catalyze the acylation of the actinoplanic polyketide with aconityl moiety in the absence of AplF activity. Thus, the aconitate must be associated with PCP of the AplD at some point to allow this outcome. Complete loss of acylation observed with the inactivation of AplD (Fig. 4*A*) confirms the criticality of the A domain and PCP of this protein, thereby offering a clue on the activation mechanism for the free TCA starting block as well as providing a plausible substrate for the AplF.

Therefore, we propose that the most likely order of events in the actinoplanic acid biosynthesis is as follows: the aconitate is loaded to the PCP of AplD via adenylation and reduced by action of AplF to form tricarballyl-PCP, which is then used for acylation of the PKS product by AplE, resulting in **5** and **6** (Fig. 3*B*). In this scenario, **11** and **12** are only shunt products unique to the *aplF* mutant and not intermediates in the pathway. A similar conclusion was made for the tetradehydro analogues of fumonisins (12).

Although the mechanism of post-PKS acylation in biosynthesis of fumonisin and actinoplanic acids seems strikingly similar, significant evolutionary distances between the involved pathways suggest a convergent evolution of this biochemistry. In addition to distances observed between the condensation domains of both ester-forming NRPSs, this is also reflected in the fact that Fum7 is a member of the iron-containing alcohol dehydrogenases (12), whereas AplF is a short-chain reductase/dehydrogenase. Given the rarity of natural products containing tricarballylic acid and the peculiarity of the enzymology, the above is a noteworthy observation.

CYP450 monooxygenase Apl3 makes the first step toward the lactonized actinoplanic acids

A putative P450 hydroxylase gene, *apl3*, was found upstream of the core PKS genes. The genetic organization suggests an independently transcribed gene, lacking the often adjacently encoded ferredoxin. In-frame deletion of *apl3* resulted in complete absence of actinoplanic acids **1**, **2**, **3**, and **4** with concomitant appearance of actinoplanic acids B and D (**5** and **6**), indicated by separate peaks with *m*/*z* $[M + NH_4]^+$ 968.5 and 954.5, respectively, in the usual 5:1 ratio (Fig. 5*B*). HRMS confirmed the identity of **5** and **6**, whereas their alkaline hydrolysis yielded **7** and **8** (Fig. S7). Complementation of the mutation with chromosomally integrated *apl3* under the control of p*ermE** resulted in partial reversion of the phenotype (Fig. S12). The

formation of the hydroxyl group of carbon 36 and, subsequently, the ability to form lactonized species of actinoplanic acids are therefore dependent of the function of this gene.

The order of events in the pathway is indicated by the absence of core polyketide intermediates hydroxylated at position 36 in the cultures of *aplD* deletion mutant, suggesting that the hydroxylation is carried out only after the acylation of the PKS backbone. In other words, the hydroxyl group must be introduced only after the formation of **5** and **6**. Given the structural similarity of these compounds with **11** and **12**, which accumulate in the *aplF* mutant, it is surprising that the latter are not hydroxylated further by the action of Apl3. It is unlikely that the *aplF* mutation would have a polar effect on *apl3* expression because the genes are located at the opposite sides of the gene cluster (Fig. 2). Indeed, reappearance of actinoplanic acids **1** and **2** upon in *trans* complementation of the *aplF* mutation (Fig. S11) confirms that Apl3 is active in this mutant. Considering all the above, it is possible that the structural differences imposed by the aconityl side chains, albeit relatively distal to the hydroxylation position, are the cause for the inability of **11** and **12** to serve as a substrate for Apl3.

Hydroxylated, open-chain derivatives **3** and **4**, which were found in the culture broth of WT *S. rapamycinicus* in significantly higher amount compared with **5** and **6** (Fig. 5*B*), indicate that lactonization rather than hydroxylation is the limiting step in the pathway. In contrast, *Actinoplanes* sp. MA7066 was reported to produce a mixture of actinoplanic acids A and B (**1** and **5**), whereas the *Streptomyces* sp. MA7099 produced exclusively actinoplanic acid B under the conditions used in the study by Singh *et al.* (3). It is not clear at this time how the closing of the double-lactone ring occurs; however, it is plausible that one of the conserved, cluster-encoded α/β-fold hydrolases/acylases (AplG or Apl4) has a role in this reaction.

APL gene cluster is colocalized with the rapamycin cluster

In the genomic context, the APL cluster is located adjacently to the rapamycin gene cluster in *S. rapamycinicus* (Fig. 2). Although regions condensed with secondary metabolite gene clusters outside of the core of the genome are not unusual in actinomycetes, the immediate proximity of the two clusters may have a more intimate evolutionary and therefore also functional background (38). Making genome-wide searches across all major publically available bacterial genome databases (NCBI, Broad Institute, and Joint Genome Institute), we were only able to find relevant similarity hits for the APL pathway in the genomes of the three known rapamycin producers (13). Vice versa, despite the increasing number of sequenced actinobacterial genomes, the *S. rapamycinicus* ATCC 29253, *S. iranensis* HM35, and *Actinoplanes* sp. N902-109 remain the only repositories of the rapamycin pathway sequenced to date. In this respect, it would be interesting to examine the genomes of the original actinoplanic acid producers, *Streptomyces* sp. MA7099 and *Actinoplanes* sp. MA7066 (1); however, these have not been sequenced yet. As in *S. rapamycinicus*, the APL and rapamycin gene clusters are also found in immediate proximity in the *Actinoplanes* sp. genome but not in *S. iranensis* where the two clusters seem to be located at the opposite arms of the chromosome. In light of all the above, we wondered whether perhaps the conserved colocalization of the pathways was more than a mere coincidence. Based both on the gene topology and similarity results, we performed synteny analysis between genomic loci harboring the rapamycin and APL clusters of the three organisms. Although both clusters are conserved at least in their essential functionality, we found a significant difference in genetic organization of the regions surrounding the PKS genes (Fig. 2). Clearly, multiple recombination events had to occur in each of the hosts from the presumably common, ancient genetic origin to come to this situation. This leads one to consider a possible evolutionary codependence of the products of both pathways.

One indication of such codependence would be an intertwined regulation of expression of the two clusters in either synchronous or contingency mode. To study these connections, we targeted the putative transcriptional regulators of both pathways. In-frame deletion of the SARP gene found at the flank of the APL cluster of *S. rapamycinicus*, *aplR*, had no influence on the production of actinoplanic acids or rapamycin compared with the WT strain (Fig. S4C). In contrast, deletion of the *rapG* and *rapH* genes, the regulators of the rapamycin pathway (39), resulted in complete loss of rapamycin production but had no influence on the levels of actinoplanic acids (Fig. S4B). Thus, the expression control of the APL pathway as well as any regulatory relationships with the rapamycin pathway remain unresolved.

Nevertheless, under the cultivation conditions used in this study, the production of rapamycin and actinoplanic acids seems to be temporally coordinated (Fig. S13). Therefore, we examined a potential functional synergy of the two compounds. Because both rapamycin and actinoplanic acids have been shown to be active against eukaryotic targets, the TOR complexes (40) and Ras farnesyl-protein transferase (2), respectively, antifungal assays were chosen for the purpose at hand.

Actinoplanic acid A and rapamycin show strong synergism in antifungal activity

We selected three diverse fungal species, *Aspergillus fumigatus*, *Candida albicans*, and *Rhizopus oryzae*, for growth inhibition assays with rapamycin and actinoplanic acid A (**1**), the major end product of the APL pathway. The concentrations of the two compounds in the assays were kept well within the biosynthetic potential of *S. rapamycinicus* ATCC 29253, which accumulates rapamycin and **1** at ~55 and ~120 μM, respectively.

Fungal cells were embedded in agar medium along with subinhibitory concentrations of **1**. When the agar solidified, rapamycin solution was spotted on top. After incubation, growth inhibition was observed in the form of clear areas in the well. As expected, a growth inhibition activity of rapamycin (40) was observed. This activity was significantly enhanced with the addition of subinhibitory amounts of **1** (Fig. 6*A*).

To ensure that the observed synergistic activity is not due to an artifact arising from the order of compound addition, the *R. oryzae* test was repeated. This time the cells were first embedded into the agar in the presence of rapamycin, and **1** was then spotted on top. This experiment resulted in similar inhibition patterns. In addition, concentration levels of both com-

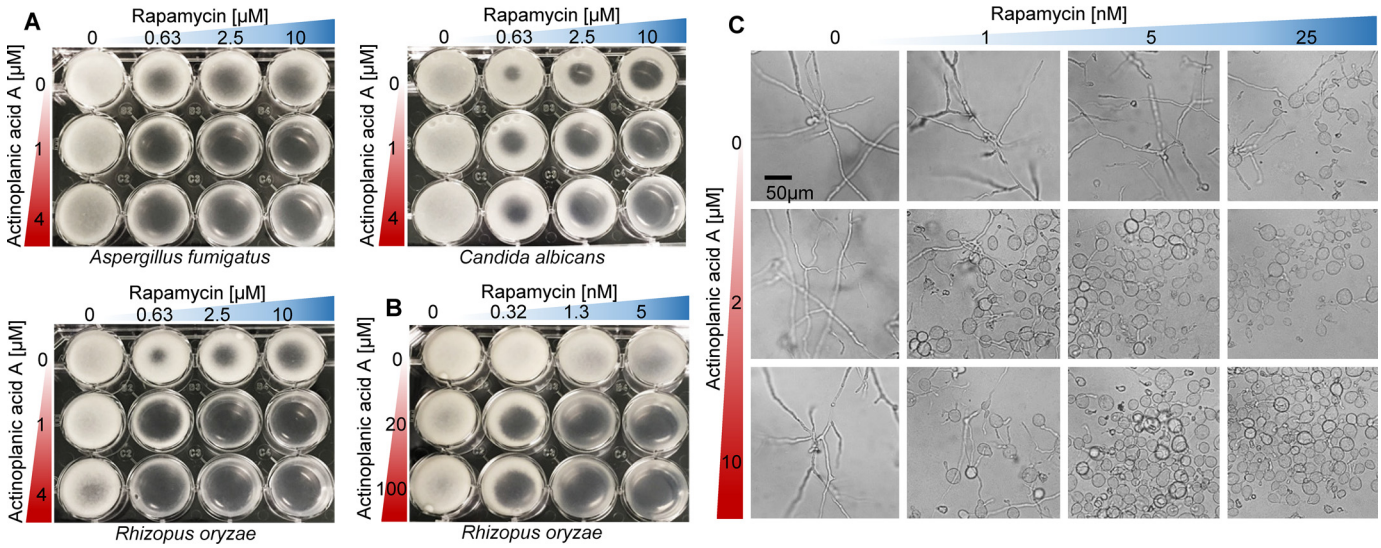

Figure 6. Synergistic antifungal activity of rapamycin and actinoplanic acid A. *A*, agar assays with *A. fumigatus*, *R. oryzae*, and *C. albicans*. Actinoplanic acid A was embedded into the PDA along with fungal cells. Rapamycin was then spotted on top. Plates were photographed after 24 h of growth. *B*, a repeated assay where first rapamycin was embedded into the PDA along with *R. oryzae* conidia, and actinoplanic acid was spotted on top of the agar. *C*, synergistic antifungal activity of rapamycin and actinoplanic acid A in PDB liquid culture. Microphotographs of *R. oryzae* conidia grown in chamber slides are shown. The photographs were taken after overnight incubation at 35 °C. Various concentrations of rapamycin and actinoplanic acid A were supplemented to the medium.

pounds were adjusted to reflect maximal subinhibitory concentrations within the assay. Although both **1** and rapamycin failed to show a clear inhibitory effect on their own, the wells with inclusion of as little as 0.32 nM rapamycin in the agar resulted in clear inhibition zones provided that **1** was present (Fig. 6*B*). It should be noted that a difference in potency of actinoplanic acid species was reported before (3). This may also hold true for the synergistic activity with rapamycin, but it remains to be tested.

To gain further insight into the effects underlying the growth inhibition observed with the initial assays, *R. oryzae* was grown in chamber slides in potato dextrose broth (PDB) supplemented with various concentrations of rapamycin and **1** (Fig. 6*C*). In agreement with the results observed in the agar tests, **1** alone, even at the highest concentration tested (10 μM), had no apparent antifungal activity. Rapamycin, however, did show partial inhibition of conidial germination but only at the highest concentration tested (25 nM). Strikingly, combining 1 nM rapamycin with 2 μM **1** resulted in close to full inhibition of *R. oryzae* spore germination. Again, the results demonstrate a clear synergistic effect of these two compounds against fungal growth. The morphological state of the exposed cultures suggests a developmental arrest; the synergy could therefore lie in the enhancement of rapamycin's mode of action. The latter is also supported by the apparent absence of antifungal activity of actinoplanic acid A alone even at relatively high concentrations (Fig. 6).

Antifungal activity of rapamycin is due to inhibition of cellular signaling through TOR complex 1 (TORC1), thereby interfering with cell cycle progression, growth, and development and with general synthesis of cellular components. Specifically, rapamycin arrests fungal cell cycle at the G_1 phase (40). Although the role of TORC1 has been investigated in relative detail, the understanding of its rapamycin-insensitive counterpart, the TORC2, is relatively poor (41). In an intertwined upstream and downstream signaling network, the two complexes coordinate processes such as protein synthesis, ribosome biogenesis, transcription, cell-cycle progression, cytoskeleton organization, stress response, and autophagy (42). Despite the wide conservation of the basic functionality throughout eukaryotes, the composition of the TOR-centered signaling network may differ significantly between various organisms (43, 44). Still, most signaling pathways upstream of the TOR complexes involve one or more small, farnesylated GTPases of the Ras superfamily. Most notably, the small G proteins Rheb, Rab, Ras, and others have been found to be involved with TOR activation in various organisms (45, 46).

Unlike the zaragozic acids, which also feature FTI activity and a tricarboxylic structural moiety (47), actinoplanic acids were found to be inert toward geranylgeranyl-pyrophosphate synthase and squalene synthase (1). Notwithstanding the possibility of an alternative mode of action, it is tempting to speculate on the plausible role of actinoplanic acids as potent and selective FTIs (1), thereby escalating the effects of rapamycin. Indeed, mutations in TOR-activating GTPases RhbI and GtrI in *C. albicans* have been shown to induce hypersensitivity to rapamycin (48, 49). In addition, synergistic antiproliferative activity of an FTI and rapamycin has been found in several mammalian cancer cell lines (50–52). Again, this was postulated to be due to inhibition of the Rheb GTPase, which normally directly activates TORC1 (46). Subsequently, several combination therapies with a rapamycin-derived drug and an FTI have been subjected to clinical testing recently (see Table S2 for the list of 34 clinical trials, including the NML identifiers). Whichever target of actinoplanic acid may prove to be valid, the mechanism of the synergetic activity with rapamycin is worthy of further investigation because the signaling network involving both TOR complexes is of principal interest to cell biologists and is a recognized target of clinical value.

Conclusions

Even well studied organisms such as *S. rapamycinicus* still hold surprises to be unveiled, in our case the biosynthesis of

actinoplanic acid and its novel analogues that lay undiscovered for over two decades. These findings led to the identification of the actinoplanic acid biosynthetic gene cluster and elucidation of the pathway sequence and biochemistry. In addition, we have provided insight into the origin of the structural diversity among the actinoplanic acid species. An important motivator for our efforts was the rare biochemistry involved with the tricarballylate group incorporated into the actinoplanic acids, the only known bacterial compounds to possess such a moiety. Our work provides an outline of the second example of this biochemistry in addition to the well examined fungal fumonisins. The core of the pathway comprises a hybrid PKS–NRPS system, which is perhaps counterintuitive at first glance due to the absence of amide bonds in the actinoplanic acid structure. Interestingly, the divergent NRPS catalyzes the formation of esters between the tricarballylic moieties and the unmodified product of the PKS. It is surprising to see that despite the clear evolutionary distances and rarity of the chemistry involved, there is a close resemblance between the fumonisin and actinoplanic acid pathways, suggesting convergent evolution of the two systems.

Furthermore, the evolutionary connection reflected in the conserved cohabitation of biosynthetic clusters for rapamycin and actinoplanic acids invited us to explore the synergism between two secondary metabolites produced by a single organism. It is increasingly evident that in their natural environment secondary metabolites produced by one organism often act in unison against multiple targets on the same foe, and so one of the paths toward network pharmacology (54) may lead from this unexpected source. Rapamycin, first isolated for its relatively weak antifungal properties, can now perhaps be better appreciated in the context of its partner, actinoplanic acid A, as a potent "one-two punch" antifungal assault. This combination attack is of course not unique. One of the most widely used anti-infectives today for example, the amoxicillin–clavulanic acid combination antibiotic drug (55), has its ancient blueprint in nature. The genome of the producer of clavulanic acid, the actinomycete *Streptomyces clavuligerus*, encodes adjacent, coregulated biosynthetic gene clusters for a β-lactam antibiotic, β-lactamase inhibitor pair, cephamycin C and clavulanic acid (56). This genetically imprinted functional synergy of the two secondary metabolites makes perfect sense, both in evolutionary and ecological aspects (38), as it increases the potency of the attack and therefore gives a competitive advantage to the host (Fig. 7*A*).

Despite the huge diversity in chemical space that the natural products represent, the repetitive use of similar search strategies has led to redundancy and a decline in the number of fundamentally novel therapies (57, 58). One plausible reason is that, restricted by the single-compound therapy paradigm, we have largely neglected the evolutionary events resulting in genetically conserved coharboring of natural product pathways, their coproduction, and the teachings hidden therein. The number of known synergistic relationships (38, 59) is surprisingly small, considering the thousands of discovered actinobacterial NPs (60) and the enormous arsenal of these compounds revealed by the rapid development of (meta)genomics. Nevertheless, increased interest in synergistic activity of natural products has already resulted in several successful attempts in systematic discovery of such NP pairs (59, 61–63). Many of these approaches are based on functional profiling of NP; however, few exploit evolutionary origins or ecological roles in their strategy. This is surprising because the sequence data of NP-producer genomes are one of the most widely accessible and rich resources. Unfortunately, the existing bioinformatics algorithms (64) process the secondary metabolite pathways in an isolated manner, leaving the evolutionary conservation hidden in plain sight.

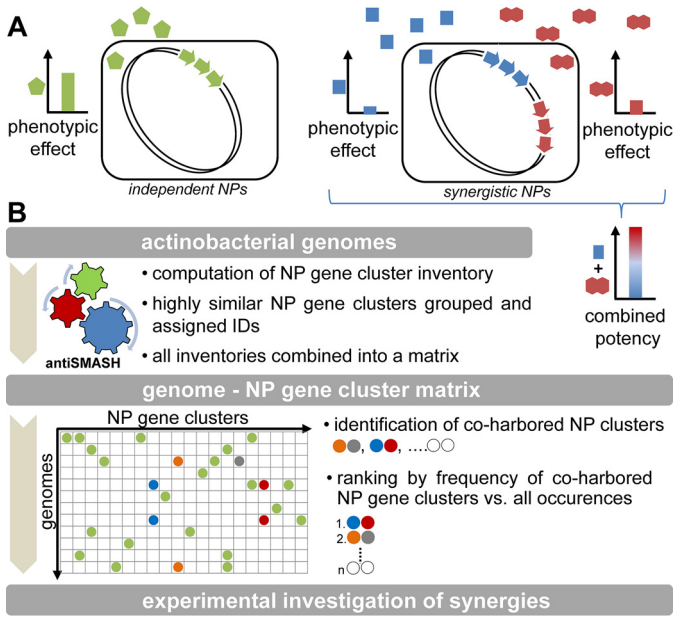

Figure 7. *A*, schematic representation of independent *versus* synergistic NP attacks. The competitive advantage for carriers of synergistic NP promotes evolutionary conservation of NP gene cluster coharboring. *B*, a possible workflow for systematic genome mining for synergistic NP based on pathway coharboring. NP gene cluster prediction was computed by antiSMASH for each genome. NP gene cluster inventories are built wherein unique IDs are assigned to groups of highly similar gene clusters. A matrix of genome–NP gene cluster inventory enables the identification of coharbored clusters and their ranking based on conservation of pathway coharboring. NP discovery efforts can then be focused on genomes harboring high-ranking pathway sets.

Thus, it may be possible to extend the search for such synergies into a wider scope with suitably adapted and systematic genome mining (Fig. 7*B*). Incidentally, this could prove to be the only practical way to address the opportunities presented by synergistic natural products when considering the enormous arsenal of these compounds revealed by the rapid development of (meta)genomics in recent years.

Experimental procedures

Strains and media

S. rapamycinicus ATCC 29253 (*S. hygroscopicus* subsp. *hygroscopicus* NRRL 5491) (65) and *S. rapamycinicus* R073, a rapamycin producer isolated from ATCC 29253, were used in this study. R073 and ATCC 29253 share 99.1% nucleotide and 98.7% CDS amino acid sequence identity over the rapamycin and APL pathway region. All manipulation on solid media was done with TAA4 agar plates (Table S3) incubated at 28 °C for 9 days. Where appropriate, apramycin (60 mg/liter) and theophylline (4 mM) were supplemented to the medium. Spores

obtained from ~1 cm^2 of the confluent, 9-day-old TAA4 agar plate culture were used as an inoculum for the shake flask fermentation. Cultures were incubated on an orbital shaker in 100-ml flasks containing 15 ml of RAP-1P medium (Table S4) at 28 °C and 260 rpm (2.5-cm throw) for 7 days. At this time, the cultures were sampled for analysis of secondary metabolites. At least three independently isolated strains were used for the phenotype characterization of genetic modifications in all cases. The sampling was performed by weighing 3 g of the culture broth diluted with 6 ml of acetonitrile:water (2:1) mixture. The samples were immediately centrifuged for 10 min at 15,000 × *g* at 4 °C. The cleared supernatants were decanted into a fresh vial and stored at −75 °C until analysis.

Genome sequencing, in silico analysis, and design

Genomic DNA was extracted from early stationary phase cultures of *S. rapamycinicus* ATCC 29253 using the method of Nikodinovic *et al*. (66). Genome sequencing was performed on the PacBio Sequel platform with sequencing library preparation performed using the SMRTbell Template Prep kit and Sequel™ Binding kit 2.0. Sequence reads were *de novo* assembled using HGAP2 software (Pacific Biosciences, Menlo Park, CA). Gene calling was performed using Prodigal software (67), and natural products pathways were annotated using antiSMASH 3.0 (16). Analysis of the biosynthetic genes was performed using BLAST algorithms (68) and Clustal Omega (69). Genetic design of constructs and single guide RNAs was performed using Geneious software (Biomatters Ltd., Auckland, New Zealand). MUSCLE (70) was also used for multiple sequence alignment. Phylogenetic trees were built using FastTree 2 (71) incorporated in the Geneious software. The newly sequenced genome of *S. rapamycinicus* ATCC 29253 has been deposited under GenBank accession number QYCY00000000.

Molecular methods

CRISPR genome editing was carried out with an in house–developed, single plasmid–based approach using pREP_P1_WTcas9 (Fig. S14). The plasmid backbone is derived from the unstable replicon, originating from pJTU412 (72), and in addition contains transfer functions (*traJ* and *oriT*) and an apramycin resistance marker (*aac(3)-IV*) from pSET152 (73). *Streptococcus pyogenes cas9* (GenBank accession number NC_002737.2, locus tag SPy_1046) was codon-optimized for expression in *Streptomyces* and put under control of the *ermE** promoter, which was fused to a theophylline riboswitch (74). Single guide RNA (17) was expressed from a gene with a synthetic P21 promoter (75), and the native *S. pyogenes* trans-activating CRISPR RNA terminator (76). Guide RNAs were designed for target homing using the integrated function of Geneious R8 (Geneious 8.1.9, Biomatters) by cross-checking for off-target potential within the genome of *S. rapamycinicus* as well as the genome of the transient host, *Escherichia coli* ET12567. The editing template was delivered on the same plasmid and typically included 500–1000-bp-long homology flanks to support double-strand break repair by homologous recombination. Both the editing template and the single guide RNA gene were synthesized by Genewiz (South Plainfield, NJ). The plasmid was delivered to the host by conjugal transfer (53) and selected for with 60 mg/liter apramycin. Exoconjugants were then subplated to agar plates containing theophylline (4 mM) to induce expression of Cas9. After incubation, colonies were transferred onto plates without antibiotic pressure and tested for the loss of apramycin resistance. Details for construction of gene inactivation CRISPR constructs are available in Table S5. Details on PCR confirmation of genotypes are listed in Fig. S15 and Table S6. Complementation experiments were performed by standard methods using the integrative pSET152 plasmid (73) with genes of interest under the control of the strong p*ermE**. Complementation vectors were assembled by taking fragments from the following genomic positions according to the deposited *S. rapamycinicus* genome, GenBank accession number CP006567.1: *aplDE*, 3155 bp (878447–881601); *apl3*, 1891 bp (9921254–9923144); and *aplF*, 930 bp (10010246–10011175).

Purification and structure elucidation of the actinoplanic acids

After 7 days of fermentation, the pH of the broth was lowered to 2.5 using hydrochloric acid. 200 g/liter Na_2SO_4 was added to facilitate extraction of fermentation products with ethyl acetate. Whole-broth extraction with 2 volumes of ethyl acetate was repeated four times. Ethyl acetate phases were pooled, dried over $MgSO_4$, and filtered. Evaporation of the solvents yielded a crude product in the form of yellow-brown oil. For purposes of structure confirmation, compounds were further purified using preparative reverse-phase (C_{18}) HPLC. This purification yielded 23.8 mg of actinoplanic acid A (**1**) and 8.2 mg of actinoplanic acid C (**2**). From a 100-liter fermenter, additionally 43.2 mg of **3** could be isolated. The structures of **1**, **2**, and **3** were determined using 1D and 2D NMR spectroscopy and comparison of the NMR data with the published data of actinoplanic acid A (2). NMR spectra were recorded on a Bruker Avance 600-MHz instrument with samples dissolved in d_6-DMSO. Alkaline hydrolysis of **9** and **10** was performed by dissolving the extract of the *aplD* deletion strain in DMSO. 100 μl of 5 M NaOH was added to 600 μl of the DMSO solution to give a pH between 13.5 and 14. The mixture was incubated for 3 h at room temperature and then neutralized with HCl. For hydrolysis of **1**, **2**, **3**, **4**, **5**, **6**, **11**, and **12**, the fermentation broth of appropriate strains was extracted with 2 volumes of methanol. 200 μl of $Ca(OH)_2$ suspension (300 g/liter in methanol) was added to 600 μl of clarified supernatant. The mixture was incubated for 3 h at 50 °C and then clarified by centrifugation.

UPLC-MS and HRMS analytics

Routine analysis of compounds in *S. rapamycinicus* cultures was performed by UPLC-MS. Clarified sample supernatant (5 μl) was injected onto an Agilent Poroshel 120 EC-C_{18} column (150 × 2.1 mm; 2.7 μm) with a flow rate of 0.9 ml/min and column temperature of 60 °C. Mobile phase A (pH 4.8) containing 10 mM ammonium formate, 0.1% formic acid, and 2% acetonitrile (v/v) and mobile phase B containing 80% acetonitrile and15% methanol (v/v) were used in the gradient profile. The method was initiated at 50% mobile phase B for the first 5 min and then progressed linearly to 73% in the next 45 min with re-equilibration to starting conditions for 3 min. MS detection was performed with an LCQ ion trap mass spectrometer (Thermo Fisher) equipped with an ESI source after a 1:1 split of the flow. Positive ionization (source voltage, 5 kV; capillary

temperature, 250 °C; sheath gas, 35 arbitrary units; auxiliary gas, 5 arbitrary units) and full-scan monitoring with m/z range 300–1000 allowed detection of the compounds, primarily as proton $[M + H]^+$ and ammonium adducts $[M + NH_4]^+$. UV diode array multiwavelength detection was performed in parallel. HRMS was performed on a Q-Exactive quadrupole/orbitrap accurate mass spectrometer (Thermo Fisher) using the same chromatographic and ionization conditions described above. The instrument was calibrated with Pierce™ LTQ Velos ESI Positive Ion Calibration Solution (Thermo Fisher) prior to the measurements. The rapamycin peak was used as an internal standard to check the accuracy of the instrument and was within ±0.3 ppm in all cases.

Antifungal assays

A. fumigatus ATCC MYA-3627, *C. albicans* ATCC 24433, and *R. oryzae* ATCC MYA-4621 were used in the antifungal assays. Conidia of *A. fumigatus* and *R. oryzae* (both harvested from a 5-day-old potato dextrose agar plate) were used as inoculum for the assays. In the case of *C. albicans*, a liquid culture with $\sim 5 \times 10^6$ cells/ml was used. Fungal cells ($\sim 1 \times 10^5$) were embedded into 1 ml of Difco potato dextrose agar (PDA; BD Biosciences) together with a DMSO solution of rapamycin and/or actinoplanic acid A. After solidifying, 2 μl of DMSO solution of the remaining compound was spotted on top of the agar. The plates were incubated at 35 °C for 24 h. Liquid culture experiments with *R. oryzae* were performed in chamber slides filled with 0.1 ml of Difco PDB (BD Biosciences) supplemented with the appropriate concentration of rapamycin and/or actinoplanic acid solution. The chambers were inoculated with $\sim 1 \times 10^4$ *R. oryzae* conidia and incubated for 16 h at 35 °C. Microphotographs were produced with an Olympus IX81 inverted microscope using a phase-contrast light source and a 20× objective lens.

Author contributions—P. M., D. P., and C. M. M. conceptualization; P. M., P. K., P. P. L., J. T., and C. M. M. data curation; P. M. and C. M. M. supervision; P. M., P. K., P. P. L., J. T., and C. M. M. investigation; P. M. visualization; P. M., P. K., P. P. L., J. T., and C. M. M. methodology; P. M., J. T., and C. M. M. writing-original draft; P. M. and C. M. M. writing-review and editing; J. T. resources.

Acknowledgments—We thank Tjaša Drčar and Eva Knapič for support with culture cultivation; Matej Ošlaj, Marko Trebušak, and Nina Pirher for assistance with the LC-MS analytics; Monika Kozlevčar and Bernarda Skok for technical assistance with genome editing; and Jerome Cluzeau for advising methods for hydrolysis of actinoplanic acids. We also thank Yue Fu for support with the antifungal assays as well as Lukas Oberer, Thomas Lochmann, and Trixie Wagner for support in NMR analytics. We thank Edward Oakeley, Ulrike Naumann, and Robert Bruccoleri for support with sequencing and assembly. We thank Frank Peterson for useful comments on this work. Special gratitude goes to Gregor Kopitar for the enthusiastic and long-standing support in every endeavor we have undertaken.

References

1. Silverman, K. C., Cascales, C., Genilloud, O., Sigmund, J. M., Gartner, S. E., Koch, G. E., Gagliardi, M. M., Heimbuch, B. K., Nallin-Omstead, M., Sanchez, M., Diez, M. T., Matrin, I., Garrity, G. M., Hirsch, C. F., Gibbs, J. B., *et al.* (1995) Actinoplanic acids A and B as novel inhibitors of farnesyl-protein transferase. *Appl. Microbiol. Biotechnol.* **43,** 610–616 CrossRef Medline
2. Singh, S. B., Liesch, J. M., Lingham, R. B., Goetz, M. A., and Gibbs, J. B. (1994) Actinoplanic acid A: a macrocyclic polycarboxylic acid which is a potent inhibitor of Ras farnesyl-protein transferase. *J. Am. Chem. Soc.* **116,** 11606–11607 CrossRef
3. Singh, S. B., Liesch, J. M., Lingham, R. B., Sileverman, K. C., Sigmund, J. M., and Goetz, M. A. (1995) Structure, chemistry, and biology of actinoplanic acids: potent inhibitors of Ras farnesyl-protein transferase. *J. Org. Chem.* **60,** 7896–7901 CrossRef
4. Saxena, N., Lahiri, S. S., Hambarde, S., and Tripathi, R. P. (2008) RAS: target for cancer therapy. *Cancer Invest.* **26,** 948–955 CrossRef Medline
5. Wang, J., Yao, X., and Huang, J. (2017) New tricks for human farnesyltransferase inhibitor: cancer and beyond. *Medchemcomm* **8,** 841–854 CrossRef Medline
6. Moorthy, N. S., Sousa, S. F., Ramos, M. J., and Fernandes, P. A. (2013) Farnesyltransferase inhibitors: a comprehensive review based on quantitative structural analysis. *Curr. Med. Chem.* **20,** 4888–4923 CrossRef Medline
7. Deepa, N., and Sreenivasa, M. Y. (2017) Fumonisins: a review on its global occurrence, epidemiology, toxicity and detection. *J. Vet. Med. Res.* **4,** 1093
8. Proctor, R. H., Desjardins, A. E., Plattner, R. D., and Hohn, T. M. (1999) A polyketide synthase gene required for biosynthesis of fumonisin mycotoxins in *Gibberella fujikuroi* mating population A. *Fungal Genet. Biol.* **27,** 100–112 CrossRef Medline
9. Proctor, R. H., Brown, D. W., Plattner, R. D., and Desjardins, A. E. (2003) Co-expression of 15 contiguous genes delineates a fumonisin biosynthetic gene cluster in *Gibberella moniliformis*. *Fungal Genet. Biol.* **38,** 237–249 CrossRefMedline
10. Gerber, R., Lou, L., and Du, L. (2009) A PLP-dependent polyketide chain releasing mechanism in the biosynthesis of mycotoxin fumonisins in *Fusarium verticillioides*. *J. Am. Chem. Soc.* **131,** 3148–3149 CrossRef Medline
11. Zaleta-Rivera, K., Xu, C., Yu, F., Butchko, R. A., Proctor, R. H., Hidalgo-Lara, M. E., Raza, A., Dussault, P. H., and Du, L. (2006) A bidomain nonribosomal peptide synthetase encoded by FUM14 catalyzes the formation of tricarballylic esters in the biosynthesis of fumonisins. *Biochemistry* **45,** 2561–2569 CrossRef Medline
12. Lia, Y., Lou, L., Cerny, R. L., Butchko, R. A., Proctor, R. H., Shen, Y., and Du, L. (2013) Tricarballylic ester formation during biosynthesis of fumonisin mycotoxins in *Fusarium verticillioides*. *Mycology* **4,** 179–186 CrossRef Medline
13. Yoo, Y. J., Kim, H., Park, S. R., and Yoon, Y. J. (2017) An overview of rapamycin: from discovery to future perspectives. *J. Ind. Microbiol. Biotechnol.* **44,** 537–553 CrossRef Medline
14. Fang, A., Wong, G. K., and Demain, A. L. (2000) Enhancement of the antifungal activity of rapamycin by the coproduced elaiophylin and nigericin. *J. Antibiot.* **53,** 158–162 CrossRef Medline
15. Baranasic, D., Gacesa, R., Starcevic, A., Zucko, J., Blazic, M., Horvat, M., Gjuracic, K., Fujs, S., Hranueli, D., Kosec, G., Cullum, J., and Petkovic, H. (2013) Draft genome sequence of *Streptomyces rapamycinicus* strain NRRL 5491, the producer of the immunosuppressant rapamycin. *Genome Announc.* **1,** e00581–13 CrossRef Medline
16. Ran, F. A., Hsu, P. D., Wright, J., Agarwala, V., Scott, D. A., and Zhang, F. (2013) Genome engineering using the CRISPR-Cas9 system. *Nat. Protoc.* **8,** 2281–2308 CrossRef Medline
17. Weber, T., Blin, K., Duddela, S., Krug, D., Kim, H. U., Bruccoleri, R., Lee, S. Y., Fischbach, M. A., Müller, R., Wohlleben, W., Breitling, R., Takano, E., and Medema, M. H. (2015) antiSMASH 3.0—a comprehensive resource for the genome mining of biosynthetic gene clusters. *Nucleic Acids Res.* **43,** W237–W243 CrossRef Medline
18. Horn, F., Schroeckh, V., Netzker, T., Guthke, R., Brakhage, A. A., and Linde, J. (2014) Draft genome sequence of *Streptomyces iranensis*. *Genome Announc.* **2,** e00616–14CrossRef Medline
19. Huang, H., Ren, S. X., Yang, S., and Hu, H. F. (2015) Comparative analysis of rapamycin biosynthesis clusters between *Actinoplanes* sp. N902-109

and *Streptomyces hygroscopicus* ATCC29253. *Chin. J. Nat. Med.* **13,** 90–98 CrossRef Medline

20. Bisang, C., Long, P. F., Cortés, J., Westcott, J., Crosby, J., Matharu, A. L., Cox, R. J., Simpson, T. J., Staunton, J., and Leadlay, P. F. (1999) A chain initiation factor common to both modular and aromatic polyketide synthases. *Nature* **401,** 502–505 CrossRef Medline
21. Ladner, C. C., and Williams, G. J. (2016) Harnessing natural product assembly lines: structure, promiscuity, and engineering. *J. Ind. Microbiol. Biotechnol.* **43,** 371–387 CrossRef Medline
22. Kosec, G., Goranovič, D., Mrak, P., Fujs, S., Kuščer, E., Horvat, J., Kopitar, G., and Petković, H. (2012) Novel chemobiosynthetic approach for exclusive production of FK506. *Metab. Eng.* **14,** 39–46 CrossRef Medline
23. Haydock, S. F., Mironenko, T., Ghoorahoo, H. I., and Leadlay, P. F. (2004) The putative elaiophylin biosynthetic gene cluster in *Streptomyces* sp. DSM4137 is adjacent to genes encoding adenosylcobalamin-dependent methylmalonyl CoA mutase and to genes for synthesis of cobalamin. *J. Biotechnol.* **113,** 55–68 CrossRef Medline
24. Blažič, M., Kosec, G., Baebler, Š., Gruden, K., and Petković, H. (2015) Roles of the crotonyl-CoA carboxylase/reductase homologues in acetate assimilation and biosynthesis of immunosuppressant FK506 in *Streptomyces tsukubaensis*. *Microb. Cell. Fact.* **14,** 164 CrossRef Medline
25. Kong, F., Zhu, T., Yu, K., Pagano, T. G., Desai, P., Radebaugh, G., and Fawzi, M. (2011) Isolation and structure of homotemsirolimuses A, B, and C. *J. Nat. Prod.* **74,** 547–553 CrossRef Medline
26. Petronikolou, N., and Nair, S. K. (2015) Biochemical studies of mycobacterial fatty acid methyltransferase: a catalyst for the enzymatic production of biodiesel. *Chem. Biol.* **22,** 1480–1490 CrossRef Medline
27. Seo, H. S., Song, J. T., Cheong, J. J., Lee, Y. H., Lee, Y. W., Hwang, I., Lee, J. S., and Choi, Y. D. (2001) Jasmonic acid carboxyl methyltransferase: a key enzyme for jasmonate-regulated plant responses. *Proc. Natl. Acad. Sci. U.S.A.* **98,** 4788–4793 CrossRef Medline
28. Struck, A. W., Thompson, M. L., Wong, L. S., and Micklefield, J. (2012) S-Adenosyl-methionine-dependent methyltransferases: highly versatile enzymes in biocatalysis, biosynthesis and other biotechnological applications. *Chembiochem* **13,** 2642–2655 CrossRef Medline
29. Condurso, H. L., and Bruner, S. D. (2012) Structure and noncanonical chemistry of nonribosomal peptide biosynthetic machinery. *Nat. Prod. Rep.* **29,** 1099–1110 CrossRef Medline
30. Bloudoff, K., and Schmeing, T. M. (2017) Structural and functional aspects of the nonribosomal peptide synthetase condensation domain superfamily: discovery, dissection and diversity. *Biochim. Biophys. Acta Proteins Proteom.* **1865,** 1587–1604 CrossRef Medline
31. Du, L., and Lou, L. (2010) PKS and NRPS release mechanisms. *Nat. Prod. Rep.* **27,** 255–278 CrossRef Medline
32. Chang, C. Y., Lohman, J. R., Huang, T., Michalska, K., Bigelow, L., Rudolf, J. D., Jedrzejczak, R., Yan, X., Ma, M., Babnigg, G., Joachimiak, A., Phillips, G. N., Jr., and Shen, B. (2018) Structural insights into the free-standing condensation enzyme SgcC5 catalyzing ester bond formation in the biosynthesis of the enediyne antitumor antibiotic C-1027. *Biochemistry* **57,** 3278–3288 CrossRef Medline
33. Lin, S., Van Lanen, S. G., and Shen, B. (2009) A free-standing condensation enzyme catalyzing ester bond formation in C-1027 biosynthesis. *Proc. Natl. Acad. Sci. U.S.A.* **106,** 4183–4188 CrossRef Medline
34. Butchko, R. A., Plattner, R. D., and Proctor, R. H. (2006) Deletion analysis of FUM genes involved in tricarballylic ester formation during fumonisin biosynthesis. *J. Agric. Food. Chem.* **54,** 9398–9404 CrossRef Medline
35. Jaklitsch, W. M., Kubicek, C. P., and Scrutton, M. C. (1991) The subcellular organization of itaconate biosynthesis in *Aspergillus terreus*. *Microbiology* **137,** 533–539
36. Blank, L., Green, J., and Guest, J. R. (2002) AcnC of *Escherichia coli* is a 2-methylcitrate dehydratase (PrpD) that can use citrate and isocitrate as substrates. *Microbiology* **148,** 133–146 CrossRef Medline
37. Massengo-Tiassé, R. P., and Cronan, J. E. (2009) Diversity in enoyl-acyl carrier protein reductases. *Cell. Mol. Life Sci.* **66,** 1507–1517 CrossRef Medline
38. Challis, G. L., and Hopwood, D. A. (2003) Synergy and contingency as driving forces for the evolution of multiple secondary metabolite production by Streptomyces species. *Proc. Natl. Acad. Sci. U.S.A.* **100,** Suppl. 2, 14555–14561 CrossRef Medline
39. Kuscer, E., Coates, N., Challis, I., Gregory, M., Wilkinson, B., Sheridan, R., and Petković, H. (2007) Roles of rapH and rapG in positive regulation of rapamycin biosynthesis in *Streptomyces hygroscopicus*. *J. Bacteriol.* **189,** 4756–4763 CrossRef Medline
40. Heitman, J., Movva, N. R., and Hall, M. N. (1991) Targets for cell cycle arrest by the immunosuppressant rapamycin in yeast. *Science* **253,** 905–909 CrossRef Medline
41. Gaubitz, C., Prouteau, M., Kusmider, B., and Loewith, R. (2016) TORC2 structure and function. *Trends Biochem. Sci.* **41,** 532–545 CrossRef Medline
42. Gonzalez, S., and Rallis, C. (2017) The TOR signaling pathway in spatial and temporal control of cell size and growth. *Front. Cell Dev. Biol.* **5,** 61 CrossRef Medline
43. van Dam, T. J., Zwartkruis, F. J., Bos, J. L., and Snel, B. (2011) Evolution of the TOR pathway. *J. Mol. Evol.* **73,** 209–220 CrossRef Medline
44. Tatebe, H., and Shiozaki, K. (2017) Evolutionary conservation of the components in the TOR signaling pathways. *Biomolecules* **7,** E77CrossRef Medline
45. Khanna, A., Loftí, P., Chavan, A. J., Montaño, N. M., Bolourani, P., Weeks, G., Shen, Z., Briggs, S. P., Pots, H., Van Haastert, P. J., Kortholt, A., and Charest, P. G. (2016) The small GTPases Ras and Rap1 bind to and control TORC2 activity. *Sci. Rep.* **6,** 25823 CrossRef Medline
46. Durán, R. V., and Hall, M. N. (2012) Regulation of TOR by small GTPases. *EMBO Rep.* **13,** 121–128 CrossRef Medline
47. Bergstrom, J. D., Dufresne, C., Bills, G. F., Nallin-Omstead, M., and Byrne, K. (1995) Discovery, biosynthesis, and mechanism of action of the zaragozic acids: potent inhibitors of squalene synthase. *Annu. Rev. Microbiol.* **49,** 607–639 CrossRef Medline
48. Flanagan, P. R., Liu, N. N., Fitzpatrick, D. J., Hokamp, K., Köhler, J. R., and Moran, G. P. (2017) The *Candida albicans* TOR-activating GTPases Gtr1 and Rhb1 coregulate starvation responses and biofilm formation. *mSphere* **2,** e00477–17 CrossRef Medline
49. Tsao, C. C., Chen, Y. T., and Lan, C. Y. (2009) A small G protein Rhb1 and a GTPase-activating protein Tsc2 involved in nitrogen starvation-induced morphogenesis and cell wall integrity of *Candida albicans*. *Fungal Genet. Biol.* **46,** 126–136 CrossRef Medline
50. Melchinger, W., Zierock, L., Wehrle, B., and Marks, R. (2013) Inhibitors of farnesyltransferase and everolimus act synergistically in growth inhibition of human T-NHL cells by involvement of AMPK. *Blood* **122,** 3076
51. Cheong, J., Eom, J. I., Lee, H. W., Park, I., Kim, Y., Kim, J. S., and Min, Y. (2007) mTOR inhibitor rapamycin interacts synergistically with farnesyltransferase inhibitor FTI-277 to induce growth inhibition in human leukemia cells. *Blood* **110,** 1821
52. Niessner, H., Beck, D., Sinnberg, T., Lasithiotakis, K., Maczey, E., Gogel, J., Venturelli, S., Berger, A., Mauthe, M., Toulany, M., Flaherty, K., Schaller, M., Schadendorf, D., Proikas-Cezanne, T., Schittek, B., *et al.* (2011) The farnesyl transferase inhibitor lonafarnib inhibits mTOR signaling and enforces sorafenib-induced apoptosis in melanoma cells. *J. Invest. Dermatol.* **131,** 468–479 CrossRef Medline
53. Kieser, T., Bibb, M., Buttner, M., Chater, K., and Hopwood, D. A. (2000) *Practical Streptomyces Genetics*, 1st Ed., pp. 249–251, John Innes Foundation, Norwich, UK
54. Hopkins, A. L. (2008) Network pharmacology: the next paradigm in drug discovery. *Nat. Chem. Biol.* **4,** 682–690 CrossRef Medline
55. World Health Organization (2017) *20th WHO Model List of Essential Medicines*, 20th Ed., World Health Organization, Geneva, Switzerland
56. Paradkar, A. (2013) Clavulanic acid production by *Streptomyces clavuligerus*: biogenesis, regulation and strain improvement. *J. Antibiot.* **66,** 411–420 CrossRef Medline
57. Patridge, E., Gareiss, P., Kinch, M. S., and Hoyer, D. (2016) An analysis of FDA-approved drugs: natural products and their derivatives. *Drug Discov. Today* **21,** 204–207 CrossRef Medline
58. Pye, C. R., Bertin, M. J., Lokey, R. S., Gerwick, W. H., and Linington, R. G. (2017) Retrospective analysis of natural products provides insights for future discovery trends. *Proc. Natl. Acad. Sci. U.S.A.* **114,** 5601–5606 CrossRef Medline

59. Wambaugh, M. A., Shakya, V. P. S., Lewis, A. J., Mulvey, M. A., and Brown, J. C. S. (2017) High-throughput identification and rational design of synergistic small-molecule pairs for combating and bypassing antibiotic resistance. *PLoS Biol.* **15,** e2001644 CrossRef Medline
60. Katz, L., and Baltz, R. H. (2016) Natural product discovery: past, present, and future. *J. Ind. Microbiol. Biotechnol.* **43,** 155–176 CrossRef Medline
61. Arp, J., Götze, S., Mukherji, R., Mattern, D. J., García-Altares, M., Klapper, M., Brock, D. A., Brakhage, A. A., Strassmann, J. E., Queller, D. C., Bardl, B., Willing, K., Peschel, G., and Stallforth, P. (2018) Synergistic activity of cosecreted natural products from amoebae-associated bacteria. *Proc. Natl. Acad. Sci. U.S.A.* **115,** 3758–3763 CrossRef Medline
62. Ramón-García, S., Ng, C., Anderson, H., Chao, J. D., Zheng, X., Pfeifer, T., Av-Gay, Y., Roberge, M., and Thompson, C. J. (2011) Synergistic drug combinations for tuberculosis therapy identified by a novel high-throughput screen. *Antimicrob. Agents Chemother.* **55,** 3861–3869 CrossRef Medline
63. Mott, B. T., Eastman, R. T., Guha, R., Sherlach, K. S., Siriwardana, A., Shinn, P., McKnight, C., Michael, S., Lacerda-Queiroz, N., Patel, P. R., Khine, P., Sun, H., Kasbekar, M., Aghdam, N., Fontaine, S. D., *et. al.* (2015) High-throughput matrix screening identifies synergistic and antagonistic antimalarial drug combinations. *Sci. Rep.* **5,** 13891 CrossRef Medline
64. Ziemert, N., Alanjary, M., and Weber, T. (2016) The evolution of genome mining in microbes—a review. *Nat. Prod. Rep.* **33,** 988–1005 CrossRef Medline
65. Kumar, Y., and Goodfellow, M. (2008) Five new members of the *Streptomyces violaceusniger* 16S rRNA gene clade: *Streptomyces castelarensis* sp. nov., comb. nov., *Streptomyces himastatinicus* sp. nov., *Streptomyces mordarskii* sp. nov., *Streptomyces rapamycinicus* sp. nov., and *Streptomyces ruanii* sp. nov. *Int. J. Syst. Evol. Microbiol.* **58,** 1369–1378 CrossRef Medline
66. Nikodinovic, J., Barrow, K. D., and Chuck, J. A. (2003) High yield preparation of genomic DNA from *Streptomyces*. *BioTechniques* **35,** 932–934, 936 CrossRef Medline
67. Hyatt, D., Chen, G. L., Locascio, P. F., Land, M. L., Larimer, F. W., and Hauser, L. J. (2010) Prodigal: prokaryotic gene recognition and translation initiation site identification. *BMC Bioinformatics* **11,** 119 CrossRef Medline
68. Altschul, S. F., Gish, W., Miller, W., Myers, E. W., and Lipman, D. J. (1990) Basic local alignment search tool. *J. Mol. Biol.* **215,** 403–410 CrossRef Medline
69. Sievers, F., Wilm, A., Dineen, D., Gibson, T. J., Karplus, K., Li, W., Lopez, R., McWilliam, H., Remmert, M., Söding, J., Thompson, J. D., and Higgins, D. G. (2011) Fast, scalable generation of high-quality protein multiple sequence alignments using Clustal Omega. *Mol. Syst. Biol.* **7,** 539 CrossRef Medline
70. Edgar, R. C. (2004) MUSCLE: multiple sequence alignment with high accuracy and high throughput. *Nucleic Acids Res.* **32,** 1792–1797 CrossRef Medline
71. Price, M. N., Dehal, P. S., and Arkin, A. P. (2010) FastTree 2—approximately maximum-likelihood trees for large alignments. *PLoS One* **5,** e9490 CrossRef Medline
72. Sun, Y., He, X., Liang, J., Zhou, X., and Deng, Z. (2009) Analysis of functions in plasmid pHZ1358 influencing its genetic and structural stability in *Streptomyces lividans* 1326. *Appl. Microbiol. Biotechnol.* **82,** 303–310 CrossRef Medline
73. Bierman, M., Logan, R., O'Brien, K., Seno, E. T., Rao, R. N., and Schoner, B. E. (1992) Plasmid cloning vectors for the conjugal transfer of DNA from *Escherichia coli* to *Streptomyces* spp. *Gene* **116,** 43–49 CrossRef Medline
74. Rudolph, M. M., Vockenhuber, M. P., and Suess, B. (2013) Synthetic riboswitches for the conditional control of gene expression in *Streptomyces coelicolor*. *Microbiology* **159,** 1416–1422 CrossRef Medline
75. Siegl, T., Tokovenko, B., Myronovskyi, M., and Luzhetskyy, A. (2013) Design, construction and characterisation of a synthetic promoter library for fine-tuned gene expression in actinomycetes. *Metab. Eng.* **19,** 98–106 CrossRef Medline
76. Deltcheva, E., Chylinski, K., Sharma, C. M., Gonzales, K., Chao, Y., Pirzada, Z. A., Eckert, M. R., Vogel, J., and Charpentier, E. (2011) CRISPR RNA maturation by trans-encoded small RNA and host factor RNase III. *Nature* **471,** 602–607 CrossRef Medline